Numerical Simulation of Hydrodynamics Characteristics in a Tank with an Up-down Reciprocating Agitator

L. C. Li[†] and B. Xu

Key Laboratory of Testing Technology for Manufacturing Process of Ministry of Education, Southwest University of Science and Technology, Mianyang, Sichuan 621010, China

†Corresponding Author Email: liliangchao@swust.edu.cn

ABSTRACT

The hydrodynamics characteristics in a tank with an up-down reciprocating disc agitator were numerically investigated using computational fluid dynamics (CFD) simulations. A dynamic mesh technique along with a user-defined function (UDF) was used to solve the reciprocating movement of the disc agitator in the tank. The dynamic flow field and averaged values of some important parameters were obtained. The verification of the simulation was completed by comparing its results with experimental data in the literature. It is found that the flow pattern in the tank with a reciprocating agitator is characterized by two dynamic vortices, which are above and below the disc, respectively. Flow field, force acting on the disc and power requirement change periodically in the tank. The increase of frequency, amplitude and disc diameter leads to the increase of the averaged velocity in the tank as a whole. Nevertheless, the uniformity of velocity distribution is slightly improved, worsened and greatly improved respectively under the above operating conditions. The averaged values of the force acting on the disc and power consumption are in the second and the third power relations with the reciprocating frequency and amplitude, respectively. The ratio of fluid averaged velocity in one cycle to averaged disc speed, and Newton number are hardly affected by reciprocating frequency and amplitude, while they increase with the enlarged size of the disc agitator.

Keywords: Mixing tank; Reciprocating agitator; Dynamic flow field; Power consumption; CFD simulation.

NOMENCLATURE

A	amplitude	$\bar{u}(t)$	instantaneous area-weighted averaged velocity
A'	total area of meshed facets		
A_0	projected area of disc in moving direction	$\tilde{u}(t)$	instantaneous arithmetic averaged velocity
D	disc diameter	$\bar{U}$	averaged velocity in one cycle in the tank
D_h	width of gap between disc and sidewall	z	disc position
f	reciprocating frequency	z_0	axial location in the tank
$F(t)$	instantaneous force acting on the disc	δ_{ij}	Kronecker delta
h	off-bottom clearance of disc	μ	molecular viscosity
H	liquid level in the tank	μ_t	turbulent viscosity
k	turbulence kinetic energy	σ	relative standard deviation
L	length of connecting-rod	ρ	density
n	total number of facts		
Ne_v	Newton number	**Abbreviations**	
p	static pressure	BDC	Bottom Dead Centre
P	power consumption	CFD	Computational Dynamic Fluid
r^*	dimensionless radial location	MU	middle position of disc moving up
Re_m	mean Reynolds number	MD	middle position of disc moving down
w	disc agitator speed	TDC	Top Dead Centre
t	time	UDF	User-Defined Function
T	cycle time		
T'	internal diameter of the tank	**Subscripts**	
u	liquid velocity	i, j	component in different directions
u_i	mean velocity of i component	**Superscripts**	
u_i'	fluctuating velocity of i component	─	averaged value of the parameter

1. INTRODUCTION

Mixing tank is a kind of common equipment, which is widely used in industrial processes. Traditional mixing tank is equipped with baffles and fluid is mixed using single or multiple rotational impellers at a constant speed. Nevertheless, traditional mixing tank has disadvantages in some situations. For instance, flow stagnant zones formed behind baffles can affect fluid mixing in the tank. The high shear rate produced by impeller rotation can cause some shear sensitive cell death in some biological processes (Brauer and Annachhrate 1992). The baffles in the tank disturb particle growth in crystallization process (Hekmat *et al*. 2007), etc.

To overcome these shortcomings of traditional mixing tank, unbaffled tank has been used as an alternative in some applications. However, the disadvantage of unbaffled tank is that fluid swirls in the tank, resulting in low mixing efficiency. Many methods have been proposed to improve the mixing efficiency, such as unsteady agitation (Frankiewicz and Woziwodzki 2022; Li and Xu 2022), eccentric agitation (Ng and Ng 2013;Takahashi *et al.* 2012) and reciprocating agitation (Hirata *et al*. 2007; Masiuk and Rakoczy 2007; Kordas *et al*. 2013; Wóziwodzki 2017; Hirose *et al*. 2022), etc. Among them, reciprocating agitation has been applied in many processes, due to its good mixing performance. It includes gas-liquid dispersion (Miyanami *et al*. 1978; Gagnon *et al*. 1998), liquid-liquid dispersion (Kamieński and Wóziwodzki 2003; Wu *et al*. 2022), solid-liquid suspension (Wóziwodzki 2014) and heat transfer (Singh *et al*. 2015). Reciprocating agitation usually uses solid discs or perforated discs to move up and down in the tank to achieve fluid mixing, which is different from that of impeller rotational agitation. Mixing efficiency and power consumption are two important parameters used to evaluate the performance of a reciprocating agitation, and some scholars have researched these in the literature. For example, Tojo *et al*. (1980) found that liquid mixing in the tank with reciprocating disc agitator is mainly controlled by turbulent mixing phenomena rather than by convective flow. Hirata *et al*. (2007) concluded that chaotic mixing along with strong turbulence caused by reciprocating agitation yields rapid mixing that is not achievable using an ordinary rotational impeller agitation. Gagnon *et al.* (1998) measured mass transfer between gas and liquid in a reciprocating plate column, and found that it was slightly better than traditional stirred tanks. Masiuk (1999) measured power consumption in a tubular vessel with a reciprocating plate agitator, and concluded that the power consumption characteristics of the reciprocating plate agitator can be described by an equation of modified power number versus Reynolds number. Kamieński and Wóziwodzki (2003) found that power input in the tank with a reciprocating agitator is a function of frequency, amplitude and disc diameter, and the effect of agitator off-bottom clearance is negligible. Wóziwodzki (2017) studied the power characteristics of reciprocating disc agitator in

laminar and fully turbulent flow regimes, and found which are similar to those of classical rotational impellers.

The mixing characteristics are closely related to flow field in the tank. Flow field and power consumption in traditional tanks with rotational impeller are relatively stable, and many scholars have studied these in the literature (Montante *et al*. 1999; Youcefi *et al*. 2013; Li *et al*. 2020; Dai *et al*. 2022). Nevertheless, flow field and power consumption in a tank with reciprocating agitator change all the time, which are much more complex than those in a traditional mixing tank. To the authors' knowledge, few scholars (Wójtowicz and Paszkowska 2015) have experimentally studied flow field in a tank with reciprocating agitator. In addition to experimental methods, computational fluid dynamics (CFD) simulation is also an important method used to study hydrodynamics in mixing tanks. It has been verified that CFD method can predict flow field and power consumption successfully in mixing tanks (Mical *et al*. 1999; Kumaresan and Joshi 2006; Fan *et al*. 2007; Hoseini *et al*. 2021; Iyer and Patel 2022). In the literature, some scholars (Komoda *et al.* 2001; Wójtowicz 2017; Orlewski *et al.* 2018) have researched flow field in tanks with reciprocating agitator. To further design and optimize the tank with reciprocating agitator, it is necessary to study in detail about the hydrodynamics characteristics in the tank. Thus, in this work, the dynamic flow field and power consumption in a tank with an up-down reciprocating agitator were researched using computational fluid dynamics (CFD) simulations.

2. NUMERICAL MODELS AND SIMULATION METHODS

2.1 Simulation Domain

Figure 1 shows the scheme of the agitated tank and its drive system. It consists of a flywheel, a connecting-rod, a vibrating-rod, a disc agitator and a cylindrical tank. The flywheel rotates to drive the disc agitator to do up-down reciprocating movement in the cylindrical tank (internal diameter $T' = 0.286$ m) for fluid mixing. Three circular flat solid discs with diameters of D_1=0.204m, D_2=0.22m and D_3=0.238m and thickness of 0.003m were used as agitators to mix the fluid. The middle height of the reciprocating disc agitator in the tank is h=0.5H, and the fluid was sealed with a top cover at the liquid level of H=T'. The position of the reciprocating disc with time can be described as follows:

$$z(t) \cong A\left[1 - \cos(2\pi ft) + \frac{A}{2L}[1 - \cos(4\pi ft)]\right]$$

(1)

The instantaneous speed of the agitator is:

$$w(t) = \frac{dz}{dt} \cong 2\pi Af\left[\sin(2\pi ft) + \frac{A}{2L}\sin(4\pi ft)\right]$$ (2)

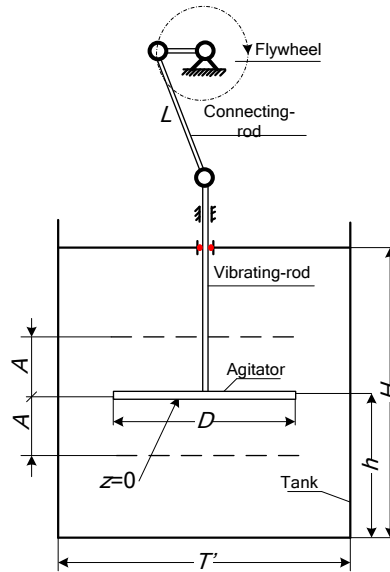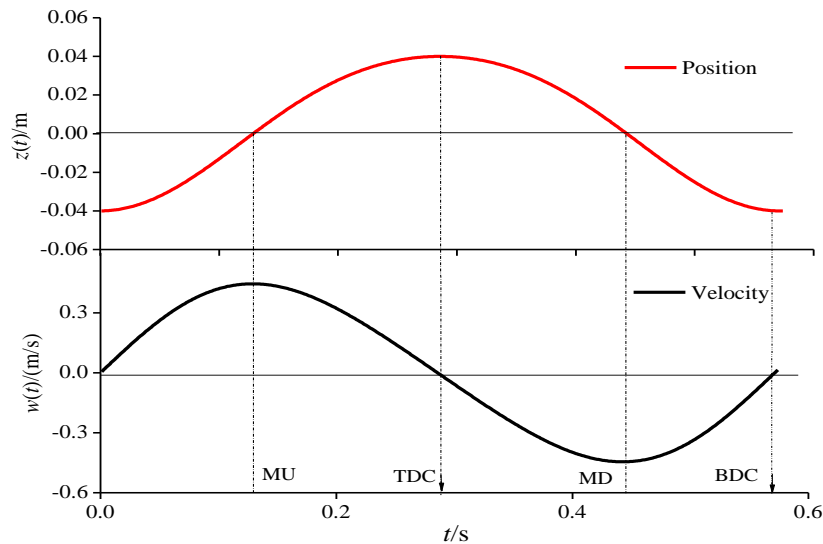**Fig. 1. Scheme of the tank and its drive system.**

Fig. 2. Instantaneous position and speed of the reciprocating agitator (A=0.04m, f=1.75Hz, L=0.25m).

where A is amplitude, varying from 0.03 to 0.06m. f is reciprocating frequency, varying from 1.75 to 2.5Hz. L is the length of connecting-rod with value of 0.25m.

Figure 2 presents the instantaneous speeds and positions of the agitator in one cycle (A=0.04m, f=1.75Hz, L=0.25m) according to Eqs. (1) ad (2). It can be seen that the instantaneous disc speed is zero at the position of bottom dead centre(BDC) and top dead centre(TDC), while the speed reaches the maximum at the middle position of disc upward motion(MU) as well as disc downward motion(MD).

2.2 Governing Equations

The instantaneous flow fields in the tank were simulated by solving the standard Navier-Stokes equation using a Reynolds averaging (RANS) approach. The continuity and momentum transport equations included in the Navier-Stokes model can be written respectively as:

Continuity equation

$$\frac{\partial \rho}{\partial t} + \frac{\partial \rho u_i}{\partial x_i} = 0 \tag{3}$$

Momentum equation

$$\frac{\partial(\rho u_i)}{\partial t} + \frac{\partial(\rho u_i u_j)}{\partial x_j} \tag{4}$$

$$= -\frac{\partial p}{\partial x_i} + \frac{\partial}{\partial x_j}\left[\mu\left(\frac{\partial u_i}{\partial x_j} + \frac{\partial u_j}{\partial x_i} - \frac{2}{3}\delta_{ij}\frac{\partial u_i}{\partial x_i}\right)\right] + \frac{\partial}{\partial x_j}(-\rho\overline{u_i' u_j'})$$

where $-\rho\overline{u_i' u_j'}$ is Reynolds stress, which can be modeled using the Bossinesq hypothesis as:

$$-\rho\overline{u_i'u_j'} = \mu_t\left(\frac{\partial u_i}{\partial x_j} + \frac{\partial u_j}{\partial x_i}\right) - \frac{2}{3}\left(\rho k + \mu_t\frac{\partial u_k}{\partial x_k}\right)\delta_{ij} \qquad (5)$$

where μ_t and k represent turbulent viscosity and turbulent kinetic energy, respectively, and can be obtained by solving a turbulence model. Wójtowicz (2017) investigated the flow regime for vibro-mixing using a mean Reynolds number Re_m, and found that fluid flow is in turbulent flow regime in the tank when $Re_m > 1000$. The mean Reynolds number for vibro-mixing is calculated as:

$$Re_m = \frac{\overline{w}D\rho}{\mu} \qquad (6)$$

$$\overline{w} = 4Af \qquad (7)$$

In this work, the minimum mean Reynolds number is 4.97×10^4, so it is in the turbulent flow regime. Then, a standard k-ε turbulence model was applied to describe the fluid fluctuations in the tank. The details of the k-ε turbulence model can be found in the literature (Launder and Spalding 1972; Launder, *et al.* 1972).

2.3 Numerical Details

As shown in Fig. 1, the tank is an axisymmetric geometry. Thus, a two-dimensional (2D) axisymmetric geometrical model was created using a CFD pre-processor Gambit 2.4.6 (Fluent Inc., 2006) to reduce the amount of calculation in the simulations. Furthermore, structured quadrilateral grids were used to divide the fluid domain of the tank (See Fig.3). The grid density independency test was conducted by monitoring instantaneous power consumption in the tank with different grid numbers during simulations. For the tank with disc diameter of 0.238m, three grid lengths, i.e., 1.5mm, 2.0mm and 3.0mm were used to conduct the grid independence verification. Through the analysis of the simulation results, the grid length of 2.0mm, and the corresponding grid number of 9975 was used as the grid size for the case. Finally, the number of grids within the range of 9950 to 11000 was used for all the cases in this study.

A CFD solver Ansys Fluent 18.0 was applied to carry out the numerical simulations. The reciprocating motion of the disc was simulated using a dynamic mesh technique. The instantaneous disc agitator speed (Eq.2) was firstly programed using the dynamic mesh define macros of "DEFINE_CG_MOTION", provided by Ansys Fluent 18.0. Then, the program was compiled and loaded onto Ansys Fluent 18.0 using a user-defined function (UDF). A dynamic layering mesh method was used to update the mesh on the dynamic zone based on the disc agitator motion. It was also important to define the boundary conditions in the simulation using the dynamic mesh technique. The agitator was defined as a rigid body, moving at speeds given by UDF. Top wall and bottom wall were defined as stationary walls. The sidewall and shaft were defined as deformed walls, since these.
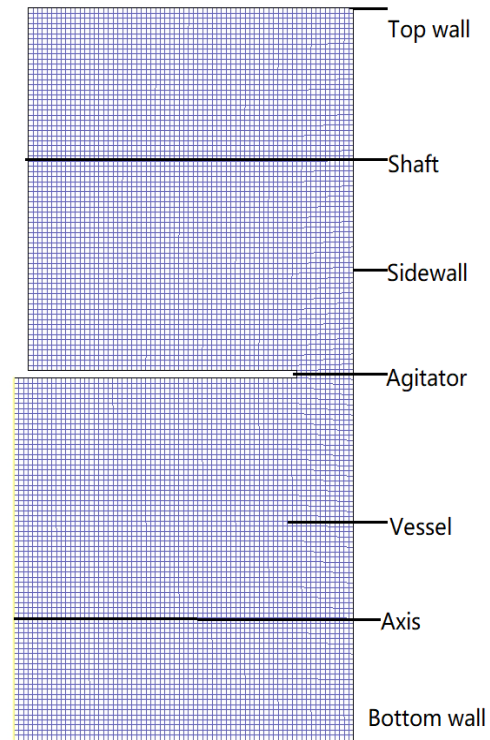

Fig. 3. Grid division for fluid domain of the tank.

walls deformed all the time during the movement of the disc agitator

The transient calculation was performed with time step of 0.001s and 20 iterations per step. The conservation equations were iteratively solved using a pressure-based solver, and a SIMPLE algorithm was used for pressure-velocity coupling. The first-order upward scheme was adopted in the discretization of the convection terms. At the initial moment, the fluid is still in the tank, and the disc is at the position of BDC. After about three cycles of the disc reciprocating movement, the flow field in the tank is no longer affected by the initial conditions. Thereupon, dynamic flow field and power characteristics in the tank after three cycles of the disc reciprocating movement were studied in the following sections.

2.4 Parameter Evaluation

Velocity and power consumption in the tank change all the time with the movement of the agitator. Also, the velocity distribution is uneven and the variation of the flow field with time in the whole tank could not be characterized by fluid velocity at a certain position. Then, as another research scheme, the averaged velocity and the uniformity of the velocity distribution in the whole tank at each moment were investigated in this work. The area-weighted averaged instantaneous velocity in the whole tank was computed as:

$$\overline{u}(t) = \frac{1}{A'}\int u(t)dA' \qquad (8)$$

where $u(t)$ is local instantaneous velocity on a meshed facet. dA' is area of the meshed facet and A' is total area of meshed facets.

A relative standard deviation(RSD) was used to evaluate the uniformity of the velocity distribution at a moment in the whole tank as:

$$\sigma(t) = \frac{\sqrt{\dfrac{\sum\limits_{i=1}^{n}(u(t)-\tilde{u}(t))^2}{n}}}{\tilde{u}(t)} \tag{9}$$

$$\tilde{u}(t) = \frac{\sum\limits_{i=1}^{n}u(t)}{n} \tag{10}$$

where n is the total number of meshed facets. The smaller the relative standard deviation, the more uniformed is the velocity distribution in the tank.

The averaged velocity and averaged relative standard deviation in one cycle in the whole tank were calculated as:

$$\bar{U} = \frac{1}{T}\int_0^T \bar{u}(t)dt \tag{11}$$

$$\bar{\sigma} = \frac{1}{T}\int_0^T \sigma(t)dt \tag{12}$$

The instantaneous force acting on the disc agitator in the direction of movement was obtained by integrating fluid pressure $p(t)$ on the surface of the disc as:

$$F(t) = \iint\limits_{A_0} p(t)dA_0 \tag{13}$$

where A_0 is projected area of the disc surface in the flow direction.

The averaged absolute force acting on the disc was calculated as:

$$\bar{F} = \frac{1}{T}\int_0^T |F(t)|dt \tag{14}$$

Then, the instantaneous power consumption and averaged power consumption were calculated as:

$$P(t) = -F(t)w(t) \tag{15}$$

$$\bar{P} = -\frac{1}{T}\int_0^T F(t)w(t)dt \tag{16}$$

The dimensionless Newton number Ne_v was also an important parameter used to evaluate the performance of the tank with reciprocating agitator, which was defined as:

$$Ne_v = \frac{\bar{P}}{\bar{w}^3 D^2 \rho} \tag{17}$$

The above parameters are evaluated in the following sections.

3. RESULTS AND DISCUSSION

3.1 Dynamic Flow Field in the Tank with a Reciprocating Agitator

As shown in Fig. 4, flow field in the tank changes with the reciprocating movement of the agitator. In general, the flow pattern in the tank is characterized by two dynamic vortices, which are above and below the disc agitator, respectively. The disc speed is zero when the disc is at the lowest position(BDC) ($t=0T$), while liquid velocity as a whole is relatively high in the tank at the moment. In particular, velocity is higher and vortex size is larger above the disc in comparison with those below the disc. As the disc moves upward, the fluid velocity weakens and vortex size reduces gradually to the smallest in the zone above the disc ($t=0.125T$, $0.25T$, $0.375T$ and $0.5T$). Meanwhile, a large amount of fluid flows from the zone above the disc to the zone below the disc through the gap between the disc and the sidewall. This causes high fluid velocity in near the wall region below the disc. As a result, fluid velocity and vortex intensity in the zone below the disc increase gradually to maximum values, and then decrease little by little until the disc reaches to TDC ($t=0.5T$). This is because the disc speed falls after the disc passes through the MU position. Subsequently, the disc moves from TDC to BDC ($t=0.5T$, $0.625T$, $0.75T$ and $0.875T$), and the evolution processes of flow field in the zones above and below the disc are almost opposite to those of the disc moving upward. In this way, flow field in the tank changes periodically with the reciprocating movement of the disc.

Figure 5 gives the axial distribution curves of fluid velocity ($r^*=0.92$) at different moments. For all the distribution curves, a velocity peak appears above and below the disc, respectively. There is almost an opposite change of velocity distribution when the disc moves upward, and when it moves downward. In addition, liquid velocity at this radial location ($r^*=0.92$) is relatively high. Under the operating condition of $A=0.04$m and $f=2.5$Hz, the maximum disc speed is only 0.63m/s ($w_{max}=2\pi Af$). Nevertheless, the highest peaks of upper and lower velocity are 2.81 and 1.06 times of the maximum disc speed, respectively, when the disc is at position of BDC. At $t=0.25T$, the velocity peak is about 3.4 times of the maximum disc speed.

In general, high pressure was found in the zone that was in front of the disc movement, while low pressure was behind it (See Fig. 6). Pressure is the highest at the centre of the tank right ahead of the disc movement, while it is the lowest at the vortex center of the zone behind the disc movement. Pressure at the vortex center of the zone in front of the disc movement is relatively low. The high-pressure zone and low-pressure zone appear alternately with the reciprocating movement of the disc. Similarly, the centers of vortices also move up and down in the axial direction with the reciprocating disc agitator.
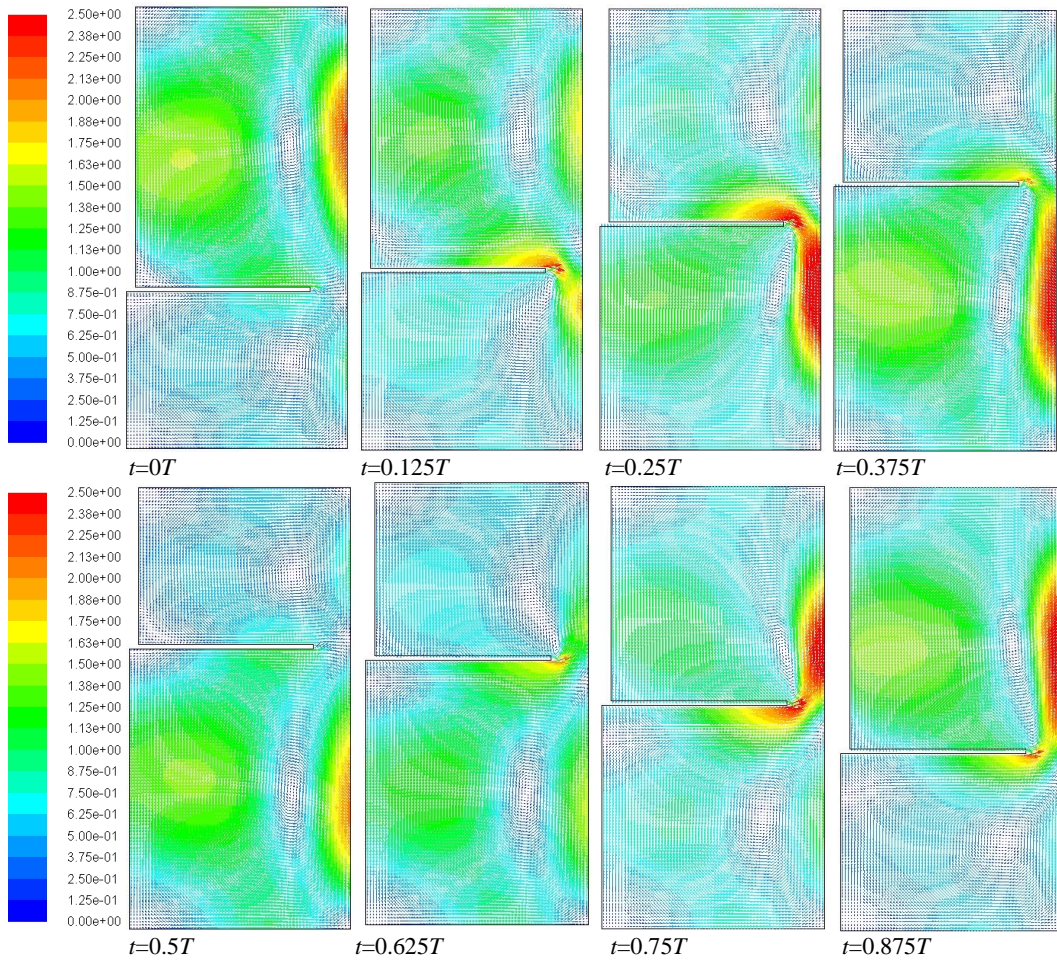
Fig. 4. Instantaneous velocity fields at different times in the tank (f=2.5, A=0.04m, D=0.238m).

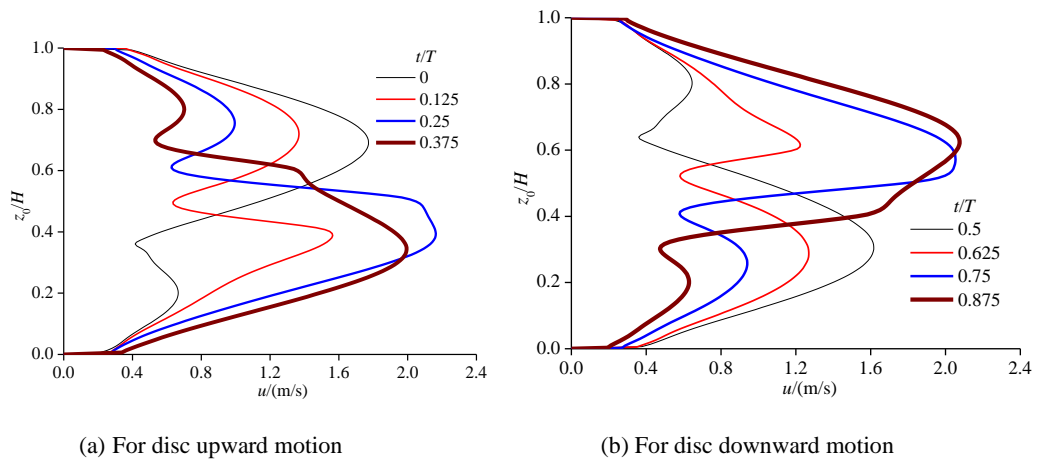(a) For disc upward motion   (b) For disc downward motion

Fig. 5. Axial distributions of resultant velocities at different times (f=2.5, A=0.04m, D=0.238m, r^*=0.92).

3.2 Effect of Reciprocating Frequency on the Dynamics Flow Field and Power Consumption

Figure 7 shows the variations of instantaneous averaged velocity in the whole tank and instantaneous relative standard deviation of velocity distribution with different reciprocating frequencies. Due to the inertia of fluid, the change of fluid velocity slightly lags behind that of disc movement (See Fig. 7(a)). For instance, the disc speed reaches the minimum value of zero at the disc position of BDC, while fluid averaged velocity in the tank is not the smallest. After a short time as the disc moves through the BDC position, the averaged velocity reaches the minimum value. With the increase of reciprocating frequency, the instantaneous averaged velocity cure rises as a whole in the tank. Nevertheless, the dimensionless averaged velocity cure was hardly affected by the frequency (See Fig. 7(b)). The simulation result
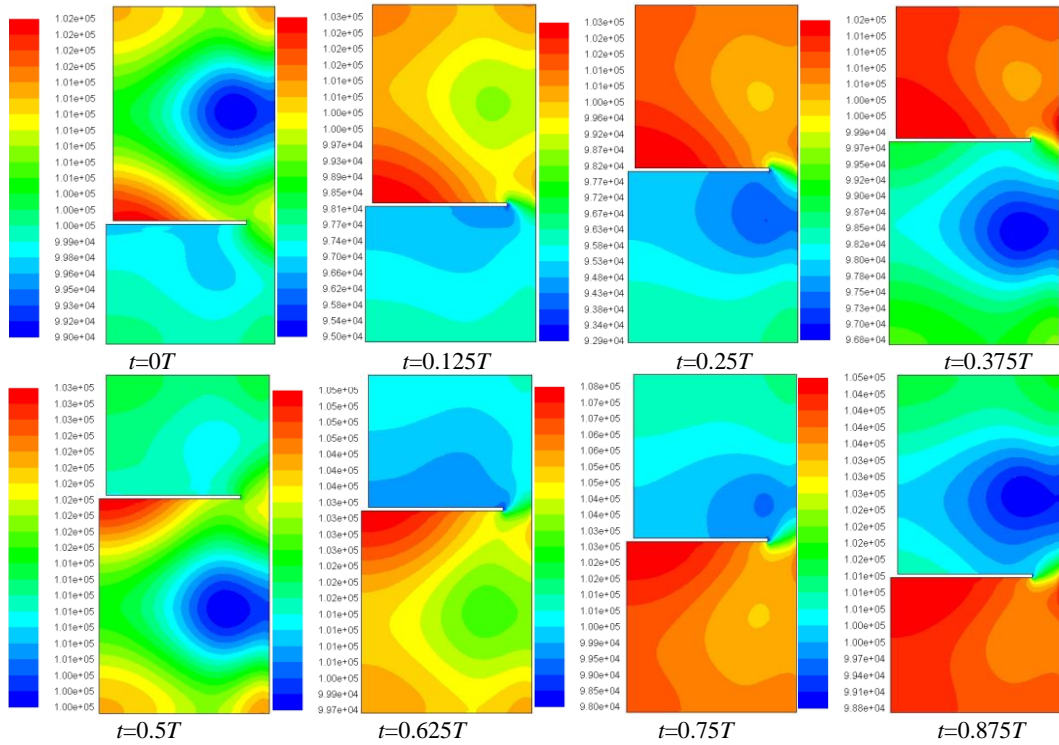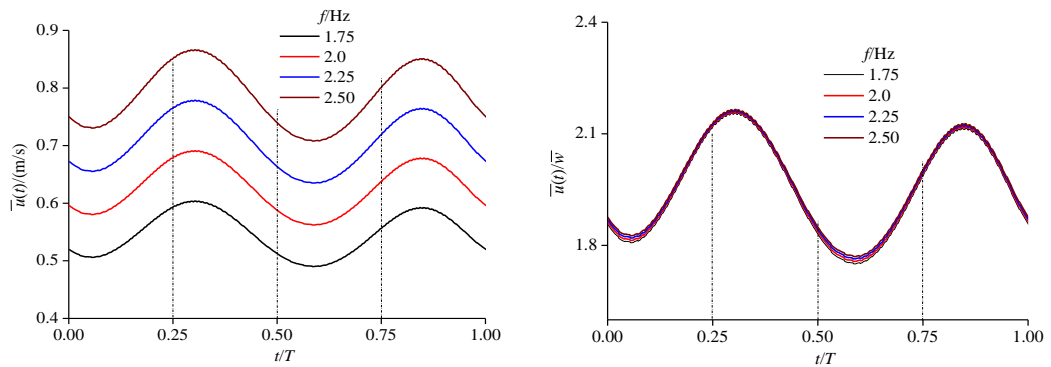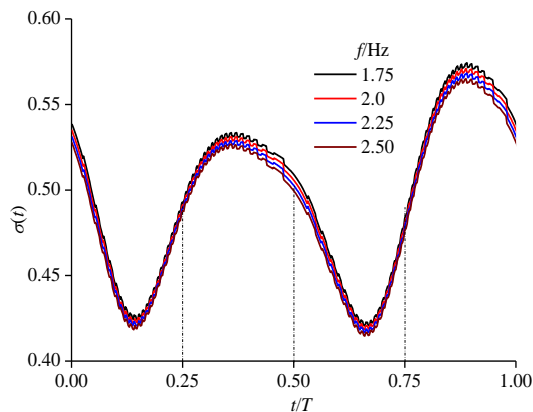
Fig. 6. Instantaneous pressure fields at different times in the tank (f=2.5, A=0.04m, D=0.238m).

(a) Averaged velocity

(b) Dimensionless averaged velocity

(c) Instantaneous relative standard deviation

Fig. 7. Instantaneous averaged velocity, dimensionless velocity and relative standard deviation with different reciprocating frequencies (A=0.04m, D=0.238m).

indicates that dynamic flow patterns in the tank do not change with the reciprocating frequency, although fluid velocity rises as a whole with increased frequency.
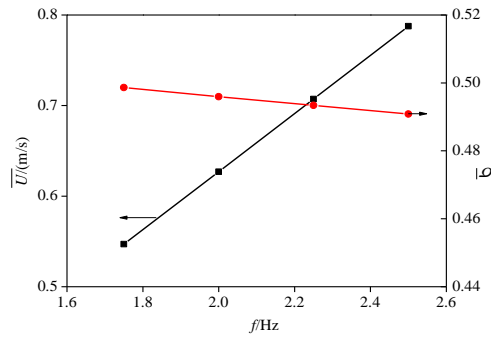
Fig. 8. Averaged velocity and relative standard deviation of different reciprocating frequencies in one cycle (*A*=0.04m, *D*=0.238m).
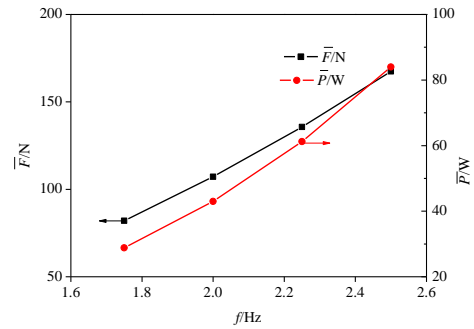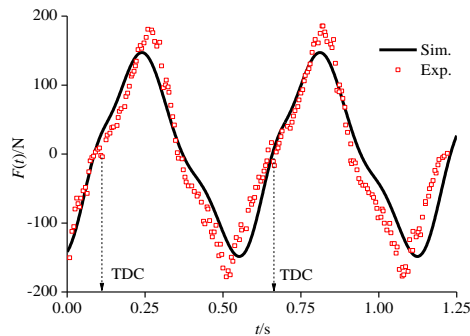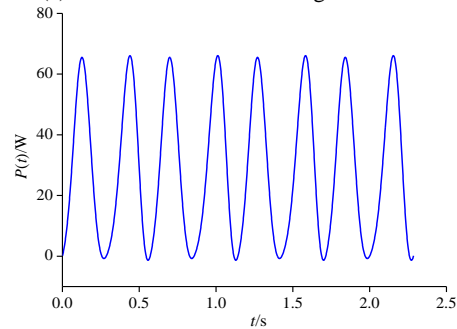

(a) Instantaneous force acting on the disc

(b) Instantaneous power consumption

Fig. 9. Instantaneous force on the agitator and power consumption in the tank.

The uniformity of velocity distribution in the tank also changes periodically, while the changing lags behind that of disc reciprocating movement (See Fig. 7(c)). In addition, the relative standard deviation cure when the disc moves upward(t=0~0.5T) is not exactly the same as when the disc moves downward (t=0.5~1.0T). This may be due to the shaft that is above the disc, which makes the structure of the zone above the disc different from that below the disc. With increase in the reciprocating frequency, the instantaneous relative standard deviation cure falls slightly as a whole. It suggests that the uniformity in the tank is improved slightly with increased frequency.

As shown in Fig. 8, the fluid averaged velocity in one cycle varies linearly with the reciprocating frequency. For a given amplitude and disc diameter, the ratio of fluid averaged velocity in one cycle to averaged disc speed $\overline{U}/\overline{w}$ is almost a constant (

Fig. 10. Averaged force and power consumption in the tank for different reciprocating frequencies.

$\overline{U}/\overline{w}$ =1.95 for *A*=0.04m and *D*=0.238m), and is hardly affected by the reciprocating frequency. The averaged relative standard deviation in one cycle falls from 0.499 to 0.491 when the frequency increases from 1.75Hz to 2.5Hz, which only decreases by 1.6%.

Figure 9 presents exemplary courses of instantaneous force acting on the disc agitator and the instantaneous power consumption in the tank. It can be observed that the instantaneous force and power consumption change periodically in the tank. The predicted force is in good agreement with the experimental data examined by Wóziwodzki (2017). Moreover, the averaged power consumption computed from Figure 9(b) is 28.82W and Newton number is 23.22, which is close to the experimental data of $\overline{P}$ =28.2 and Ne_v=22.7 in the literature (Wóziwodzki 2017) .The relative errors of $\overline{P}$ and Ne_v between the simulation results in this work and experimental data in the literature are 2.2% and 2.29%, respectively.

As shown in Fig. 10, the averaged values of force and power consumption increase with the rise of frequency. By fitting data in Fig.10, the relationship between the averaged force and frequency is about $\overline{F} \propto f^2$, and that between the averaged power consumption and frequency is about $\overline{P} \propto f^3$, respectively. However, the Newton number Ne_v remains almost unchanged with value of 23.22 for different reciprocating frequencies.

3.3 Effect of Amplitude on the Dynamic Flow Field and Power Consumption

With increase in amplitude, the instantaneous averaged velocity in the tank rises as a whole, and its dimensionless averaged velocity fluctuates more (See Fig. 11(a), (b)). Besides, the higher the instantaneous dimensionless averaged velocity, the more obvious effect amplitude has. Instantaneous relative standard deviation also increases with greater amplitude (See Fig. 11(c)). The simulation result indicates that the increase of amplitude would go against the uniformity of velocity distribution in the tank. It may be that the increase of amplitude brings the influence of reciprocating movement of
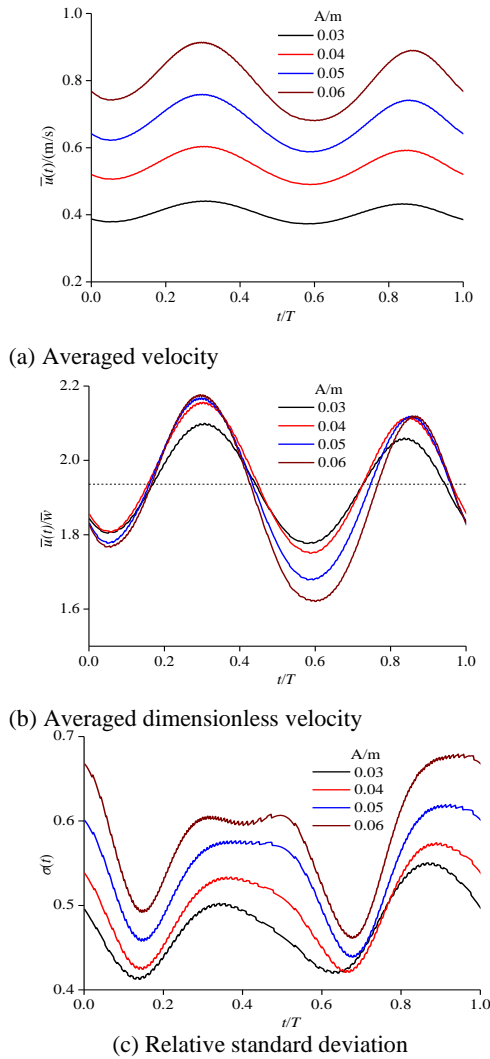
(a) Averaged velocity

(b) Averaged dimensionless velocity

(c) Relative standard deviation
Fig. 11. Instantaneous averaged velocity, dimensionless velocity and relative standard deviation with different amplitudes (f=1.75Hz, D=0.238m).

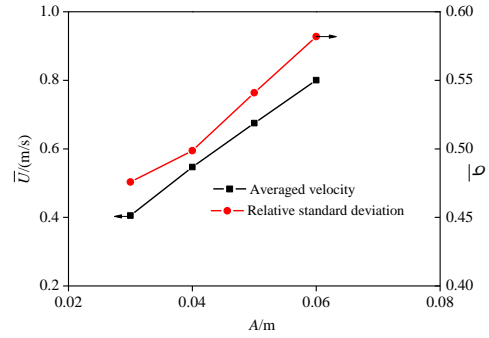**Fig. 12. Averaged velocity and relative standard deviation for different amplitude in one cycle (f=1.75Hz, D=0.238m).**
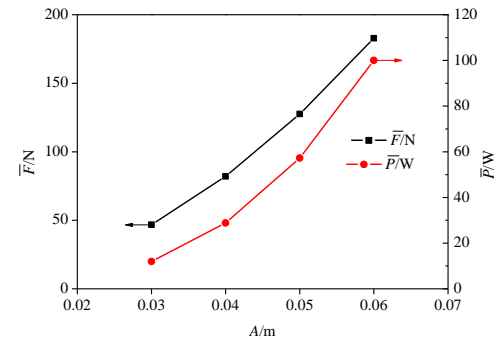

Fig. 13. Averaged force and power consumption in the tank for different amplitudes (f=1.75Hz, D=0.238m).

disc to a wider range of fluid domain, which worsens the velocity distribution in the tank.

As shown in Fig. 12, the averaged velocity in one cycle varies almost linearly with the amplitude, which is similar to the effect of frequency discussed previously. Also, the ratio of $\overline{U}/\overline{w}$ is almost a constant, and is hardly affected by amplitude at a given reciprocating frequency and disc diameter ($\overline{U}/\overline{w}$ =1.95 for f=1.75 m and D=0.238m). As analyzed above, amplitude has a great effect on the uniformity of velocity distribution in the tank, which is different from that of frequency. When amplitude increases from 0.03 to 0.06m, the averaged relative standard deviation in one cycle rises from 0.476 to 0.582; it increases by 22.3%.

It can be observed from Fig.13 that averaged force and power consumption rise with the increase of amplitude. By fitting the data in Fig.13, the relationships between amplitude and each parameter are $\overline{F} \propto A^{1.97}$, and $\overline{P} \propto A^{3.1}$, respectively. Considering the accuracy of

simulations, the averaged force should be proportional to the second power of amplitude ($\overline{F} \propto A^2$), and the averaged power consumption should be proportional to the third power of amplitude ($\overline{P} \propto A^3$). The Newton number Ne_v changes from 23.22 to 23.87 when amplitude increases from 0.03 to 0.06m, hence, Ne_v is hardly affected by amplitude.

3.4 Effect of Disc Diameter on Dynamic Flow Field and Power Consumption

As shown in Fig. 14, the diameter of disc has great effects on instantaneous averaged velocity and the uniformity of velocity distribution in the tank. With increase in the disc diameter, both instantaneous averaged velocity and instantaneous dimensionless averaged velocity rise. It can be explained that the larger the disc diameter, the narrower the gap between the disc and the sidewall of the tank is. As a result, higher velocity of fluid flows through the gap, which leads to the high velocity of fluid in sidewall regions in the tank for a large disc. Furthermore, the high velocity in near the wall regions would affect the fluid velocity in the whole tank, which makes velocity in the whole tank relatively high. The instantaneous relative standard deviation falls with the increase of the disc diameter (Fig. 14(c)). In summary, averaged velocity rises and the uniformity of velocity distribution becomes

(a) Averaged resultant velocity

(b) Dimensionless averaged velocity

(c) Relative standard deviation

Fig. 14. Instantaneous averaged velocity, dimensionless velocity and relative standard deviation with different disc diameters (A=0.04m, f=2.0 Hz).
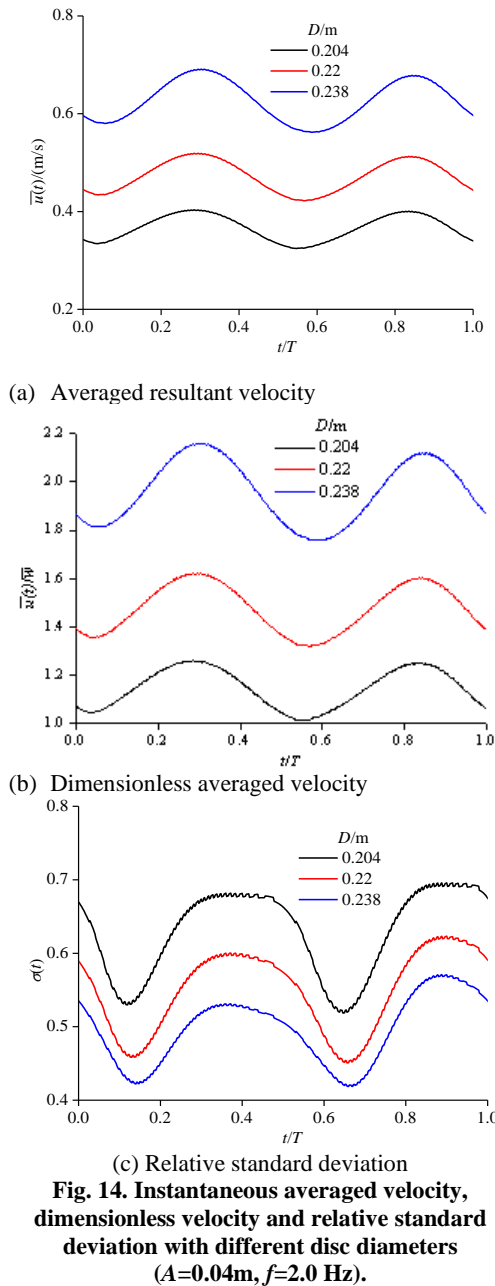
better for the large disc, which may favor fluid mixing.

Figure 15 gives the averaged velocity and relative standard deviation of velocity distribution in one cycle for different disc diameters. Consistent with the effect of disc diameter on instantaneous values of parameters, the increase of disc diameter leads the averaged velocity in one cycle to increase obviously and the relative standard deviation to decrease greatly. As previously discussed, reciprocating frequency and amplitude have little effect on the ratio of $\overline{U}/\overline{w}$. Nevertheless, the disc diameter has great effect on the ratio of $\overline{U}/\overline{w}$. In this work, the ratios of $\overline{U}/\overline{w}$ are 1.14, 1.48 and 1.95 for the disc diameters of 0.204m, 0.22m and 0.238m, respectively. The ratio increases by 71% when disc diameter varies from 0.204m to 0.238m.
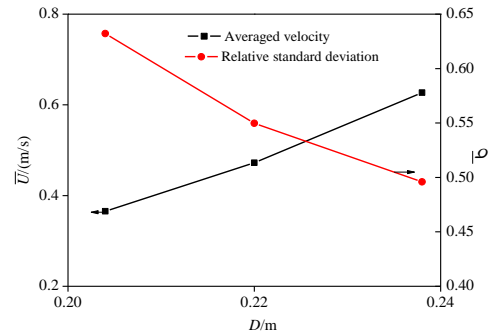

Fig. 15. Averaged velocity and relative standard deviation for different diameters of disc in one cycle (A=0.04m, f=2.0 Hz).

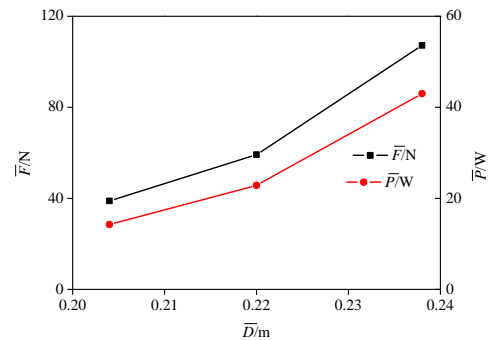**Fig. 16. Averaged force and power consumption in the tank for different disc diameters (A=0.04m, f=2.0Hz).**

As shown in Fig.16, both averaged force and averaged power consumption rise greatly with the increase of disc diameter. Within the scope of this study, the relationships between gap size (D_h=(T'-D)/2) and averaged force, and averaged power consumption are $\overline{F} \propto D_h^{-1.89}$ and $\overline{P} \propto D_h^{-2.06}$, respectively. The Newton number Ne_v rises with the gap narrowing. For the disc diameter of 0.204m, 0.22m and 0.238m, the predicted Ne_v is 10.48, 14.43 and 23.22 respectively, which is close to the experimental data measured by Wóziwodzki (2017) with values of 10.2, 15.2 and 22.7 for the corresponding disc diameters. The relative errors between the simulation results and experimental data are very small.

4. CONCLUSION

CFD simulations were carried out to study the hydrodynamics characteristics in a tank with an up-down reciprocating agitator using a dynamic mesh technique. The effects of frequency, amplitude and disc diameter were investigated in detail. The following conclusions were obtained.

(1) The flow pattern in the tank with a reciprocating agitator is characterized by two dynamic vortices, which are above and below the disc, respectively. The flow field, force acting on the disc and power consumption change periodically in the tank. The variations of instantaneous averaged velocity and uniformity of velocity distribution lag behind those of disc movement.

(2) The averaged velocity in the tank rises as a whole with increase in the reciprocating frequency, amplitude and disc diameter. However, the uniformity of velocity distribution under the above three conditions is improved slightly, worsened and improved greatly, respectively. Dynamic flow patterns in the tank do not change with frequency. The ratio of fluid averaged velocity in one cycle to averaged disc speed $\overline{U}/\overline{w}$ is hardly affected by reciprocating frequency and amplitude, while it increases with a larger disc agitator.

(3) The increase of frequency, amplitude and disc diameter would results in the greater force and higher power consumption for the disc movement. The averaged force acting on the agitator and averaged power consumption are in the second and the third power relations with the reciprocating frequency and amplitude, respectively. Newton number remains almost unchanged for the different frequencies and amplitudes, bu it increases with the enlargement of the disc diameter.

REFERENCES

Brauer, H. and A. P. Annachhrate (1992). Nitrification and denitrification in a system of reciprocating jet bioreactor. *Bioprocess Engineering* 7 (6), 269-275.

Dai, Y. X., Z. H. Wang, Y. W. Fan and Z. Q. Cheng (2022). Analysis of mixing effect and power consumption of cone-bottom dual Rushton turbines stirred tank. *Chemical Papers* 76, 2177-2191.

Fan, J. H., Y. D. Wang and W. Y. Fei (2007). Large eddy simulations of flow instabilities in a stirred tank generate by a Rushton turbine. *Chinese Journal of Chemical Engineering* 15 (4), 200-208.

Frankiewicz, S. and S. Woziwodzki (2022). Gas hold-up and mass transfer in a vessel with an unsteady rotating concave blade impeller. *Energies* 346(15), 1-15

Gagnon, H., M. Lounes and J. Thibault (1998). Power consumption and mass transfer in agitated gas-liquid columns: a comparative study. *Canadian Journal of Chemical Engineering* 76, 379-389.

Hekmat, D., D. Hebel, H. Schmid and D. Weuster-Botz (2007). Crystallization of lysozyme: from vapor diffusion experiments to batch crystallization in agitated mo-scale vessels. *Process Biochemitry* 42(12), 1649-1654.

Hirata, Y., T. Dote, T. Yoshioka, Y. Komoda and Y. Inoue (2007). Performance of chaotic mixing caused by reciprocating a disk in a cylindrical vessel. *Chemical Engineering Research & Design* 85(A5), 576-582.

Hirose, H., Y. Komoda, T. Horie and N. Ohmura (2022). Topology and dynamics of streakline on the mixing boundary of two-dimensional chaotic flow induced by a rotationally reciprocating anchor impeller. *Journal of the Taiwan Institute of Chemical Engineers* 131 (104213), 1-7.

Hoseini, S. S., G. Najafi, B. Ghobadian and A. H. Akbarzadeh (2021). Impeller shape-optimization of stirred-tank reactor: CFD and fluid structure interaction analyses. *Chemical Engineering Journal* 413 (6), 1-18.

Iyer, D. K. and A. K. Patel (2022). Physical reasoning of double-to single-loop transition in industrial reactors using computational fluid dynamics. *Journal of Applied Fluid Mechanics* 15(5), 1621-1634.

Kamieński, J. and R. Wóziwodzki (2003). Dispersion of liquid-liquid systems in a mixer with a reciprocating agitator. *Chemical Engineering and Processing* 42 (12), 1007-1017.

Komoda, Y., Y. Inoue and Y. Hirata (2001). Characteristics of turbulent flow inducted by reciprocating disk in cylindrical vessel, *Journal of Chemical Engineering of Japan* 34 (7), 929-935.

Kordas, M., G. Story, M. Konopacki and R. Rakoczy (2013). Study of mixing time in a liquid vessel with rotating and reciprocating agitator. *Industrial and Engineering Chemistry Research* 52 (38),13818-13828.

Kumaresan, T. and J. B. Joshi (2006). Effect of impeller design on the flow pattern and mixing in stirred tanks. *Chemical Engineering Journal* 115 (3), 173-193.

Launder, B. E. and D. B. Spalding (1972). *Lectures in Mathematical Models of Turbulence*. Academic Press London, England.

Launder, B. E., G. J. Reece and W. Rodi (1972). *Progress in the Development of a Reynolds-Stress Turbulence Closure*. England: Academic Press.

Li, L. C. and B. Xu (2022). CFD simulation of hydrodynamics characteristics in a tank with forward-reverse rotating impeller. *Journal of the Taiwan Institute of Chemical Engineers* 131 (104174), 1-13.

Li, L. C., N. Chen, K. F. Xiang and B. P. Xiang (2020). A comparative CFD study on laminar and turbulent flow fields in dual-Rushton turbine stirred vessels. *Journal of Applied Fluid Mechanics* 13(2), 413-427.

Masiuk, S. (1999). Power consumption measurements in a liquid vessel that is mixed using a vibratory agitator. *Chemical Engineering Journal*, 75 (3), 161-165.

Masiuk, S. and R. Rakoczy (2007). Power consumption, mixing time, heat and mass transfer measurement for liquid vessels that are mixed using reciprocating multiple agitators. *Chemical Engineering and Processing* 46, 89-98.

Mical, G., A. Brucato and F. Grisafi (1999). Prediction of flow fields in a dual impeller stirred vessel. *AIChE* 45 (3), 445-464.

Miyanami, K., K. Tojo, I. Minami and T. Yano (1978). Gas-liquid mass transfer in a vibrating disk column. *Chemical Engineering Science* 33 (5), 601-608.

Montante, G., A. Brucato, K. C. Lee and M. Yianneskis (1999). An experimental study of double-to single-loop transition in stirred vessels. *Canadian Journal of Chemical Engineering* 77, 649-659.

Ng, K. C. and E. Y. K. Ng (2013). Laminar mixing performances of baffling, shaft eccentricity and unsteady mixing in a cylindrical vessel. *Chemical Engineering Science* 104, 960-974.

Orlewski, P. M., Y. Wang, M. S. Hosseinalipour, D. Kryscio, M.Iggland and M. Mazzotti (2018). Characterization of a vibromixer: Experimental and modeling study of mixing in a batch reactor. *Chemical Engineering Research and Design* 137, 534-543.

Singh, A. P., A. Singh and H. S. Ramaswamy (2015). Modification of a static steam retort for evaluating heat transfer under reciprocation agitation thermal processing. *Journal of Food Engineering* 153, 63-72.

Takahashi, K., Y. Sugo, Y. Takahata, H. Sekine and M. Nakamura (2012). Laminar mixing in stirred tank agitated by an impeller inclined. *International Journal of Chemical Engineering* 2012, 1-10.

Tojo, K., H. Mitsui and K. Miyanami (1980). Mixing performance of vibrating disk tank. *Chem. Eng. Communications* 6 (4-5), 305-311.

Wójtowicz, R. and S. Paszkowska (2015). Investigations of liquid flow velocity in a vibromixer using stereo PIV anemometry. *Technical Transactions*.

Wóziwodzki, R (2014). Choice of an optimal agitated vessel for the drawdown of floating solids. *Industrial & Engineering Chemistry Research* 53 (36), 13989-14001.

Wóziwodzki, R (2017). Flow pattern and power consumption in a vibromixer. *Chemical Engineering Science* 172, 622-635.

Wu, Y., J. Vovers, H. T. Lu, W. Li, G. W. Stevens and K. A. Mumford (2022). Investigation of the extraction of natural alkaloids in Karr reciprocating plate columns: Fluid dynamic stuy. *Chemical Engineering Science* 264 (110890), 1-13.

Yang, F. L., C. X. Zhang, H. Y. Sun and W. P. Liu (2022). Solid–liquid suspension in a stirred tank driven by an eccentric-shaft: electrical resistance tomography measurement. *Powder Technology* 411 (117943), 1-16.

Youcefi, S., M. Bouzit, H. Ameur, Y. Kamla and A. Youcefi (2013). Effect of some design parameters on the flow fields and power consumption in a vessel stirred by a Rushton turbine. *Chemical and Process Engineering* 34(2), 293-307.